V. Cavalieri, A. De Gaspari, S. Ricci
Aero-Structural Design Optimization of a Morphing Aileron Considering Actuation Aspects
in: AIAA Scitech 2024 Forum, AIAA, 2024, ISBN: 9781624107115, p. 1-17, AIAA 2024-2113
[AIAA Scitech 2024 Forum, Orlando, FL, USA, 8-12 Jan. 2024]
doi:10.2514/6.2024-2113

Aero–Structural Design Optimization of a Morphing Aileron Considering Actuation Aspects

Vittorio Cavalieri*, Alessandro De Gaspari† and Sergio Ricci‡
Politecnico di Milano, Department of Aerospace Science and Technology, 20156 Milano, Italy

This paper summarizes the results obtained in the framework of the Clean Aviation Joint Undertaking on the development of a dedicated morphing aileron. This device, designed to be installed on the high aspect ratio wing of a hybrid–electric regional aircraft, is conceived to replace the traditional hinged aileron with an innovative aileron optimized for minimizing the actuation force and the aerodynamic drag, ensuring a smoothed and continuous skin surface. The design of such a complex device required a multi–disciplinary design approach, able to combine aerodynamic performances, kinematic and structural requirements, and actuation aspects related to the compliant structures concept on which the morphing device is based. The paper includes the description of the different design levels together with the obtained results, the selected optimal solutions, and finally a numerical validation phase.

I. Introduction

This paper describes the aerodynamic and structural design optimization of a morphing aileron in the framework of the Hybrid Electric Regional Wing Integration Novel Green Technologies (HERWINGT) project, supported by the Clean Aviation Joint Undertaking and funded by the European Union. This project contributes to the research aimed at the decarbonization of aviation systems, since it is increasingly important to mitigate the environmental impact of air transportation [1]. Different solutions are investigated to achieve a significant reduction in fuel consumption. These solutions are related to improved aerodynamic efficiency, light–weight wing structures and hybrid–electric propulsion. Among the different technologies, the morphing concept has the potential to enhance the aerodynamic efficiency, reduce pollutant emissions and noise [2], and also improve the structural efficiency. In particular, a morphing control surface can be used to reduce drag and for load alleviation. By demonstrating these capabilities, the morphing aileron becomes a valid alternative to replace the conventional hinged aileron.

From the aerodynamic perspective, the smooth curvature change achievable with morphing enables improved efficiency [3]. However, the morphing concept is a viable option only if an overall advantage is obtained [4], i.e. if, together with aerodynamics, a weight benefit is also achieved. In the case of an aileron, much of the weight comes from the actuation system. Taking advantage of the greater design freedom of morphing devices, the work presented in this article seeks to design a morphing aileron able to minimize the aerodynamic drag and, at the same time, the maximum actuation force that drives the choice of the actuation system. Therefore, the actuation aspects of the morphing aileron are considered, both as design objective and as performance index in the validation phase.

The design procedure adopted in this work embeds skin structural constraints and energetic information from the early stages of aerodynamic shape optimization. Different candidate morphing shapes characterized by reduced drag can be obtained, but they differ for the required actuation level. Therefore, the actuation aspects cannot be considered separately from the aerodynamic performances. The structural design is then performed through a dedicated multi–objective topology and sizing optimization. The aim of this optimization is the design of a structural configuration able to achieve different target shapes with minimum geometrical error and minimum actuation force.
Therefore, a multi–level approach is adopted for the optimal design of a morphing aileron based on compliant structures. The first level works on the definition of the optimal target shape taking into account structural and actuation aspects. In the next levels, an ad hoc–developed topology optimization tool is used to define the optimal structural configuration which is able, once actuated, to deform itself matching the optimal shape coming out from the first level [5, 6]. After a description of the initial design requirements and the adopted morphing aileron concept in Section II, the first level is described in Section III, while the second level is covered in Section IV. Then, the designed structural solution is validated from the aerodynamic viewpoint. Moreover, the morphing aileron is compared with an equivalently–sized

*Post–Doctoral Researcher, Politecnico di Milano, Department of Aerospace Science and Technology, via La Masa 34, 20156 Milano, Italy
†Associate Professor, Politecnico di Milano, Department of Aerospace Science and Technology, via La Masa 34, 20156 Milano, Italy
‡Full Professor, Politecnico di Milano, Department of Aerospace Science and Technology, via La Masa 34, 20156 Milano, Italy

hinged aileron from the actuation force viewpoint, to assess the overall convenience of the morphing concept. Finally, the modal analysis of the structure is reported. These assessments are discussed in Section V.

The outlined procedure has proven effective in the design of a morphing solution able to overcome the aerodynamic and actuation performances of the conventional aileron. In this paper, the procedure is applied to the morphing aileron of the regional aircraft in the framework of HERWINGT project. The design activity described in this paper represents the basis for the future realization of a full–scale demonstrator for the experimental validation of the proposed concept.

II. Initial design requirements and morphing aileron concept

The aim of the HERWINGT project is to design an innovative wing suitable for the future Hybrid Electric regional aircraft (HER) that will contribute to the overall target to reduce fuel burn, CO2 and other GHG emissions by improving aerodynamic efficiency and reducing weight. This wing design will benefit for all technologies matured during this project. Among these technologies, a morphing aileron is taken into consideration which will be designed to minimize aerodynamic drag during maneuvers and, at the same time, require less actuation force than its traditional hinged counterpart. A lower actuation force should allow the installation of a lighter actuation system.

In parallel with the development of new technologies to be integrated into the wing, other activities inside HERWINGT project are mainly focused on the definition of possible wing architectures having in mind a hypothetical reference aircraft in line with the general objectives of the project, so typically a twin prop medium range regional aircraft, with number of pax ranging from 80 to 90, and MTOW around 30000 kg.

One of the difficulties in defining the wing architecture is that it depends on the the entire aircraft architecture, which is investigated in the HERA (Hybrid Electric Regional Aircraft) project and has not yet been defined. For this reason, the wing architecture proposed by HERWINGT must be iteratively adjusted on the basis of the inputs coming from full A/C HERA project. Two different aircraft configurations are currently considered, i.e. cantilever and strut braced wing. Whatever aircraft configuration is selected, the main research objective is to increase the aspect ratio of the wing as much as possible, to maximize the reduction of induced drag, leading to a high aspect ratio wing configuration where the outer external wing shape should not change anymore. In this region, the aileron covering the last 5 m of the wing is installed, as reported in Fig. 1.

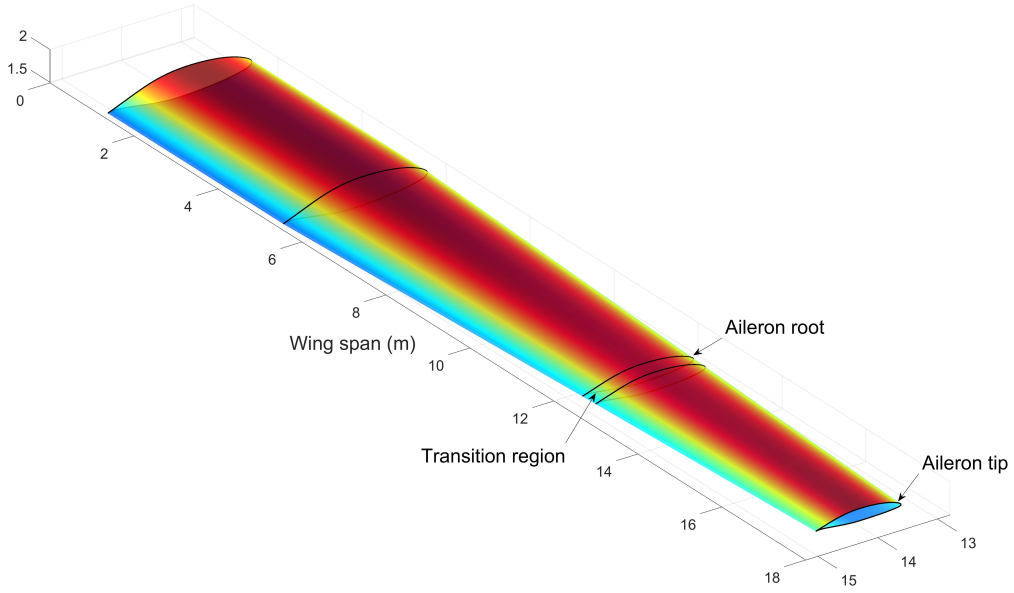

Fig. 1 Wing geometry and aileron region.

The main goal of this work is to design a morphing aileron able to work in the same flight conditions, minimizing at the same time the aerodynamic drag and the total actuation force. The initial requirements include a rear spar located at 60% of the local chord. Consistent with this information, the hinge position of the traditional aileron and the chordwise position where the morphing control surface can start its deformation were placed at the 70% of the local chord, in order to have space for positioning the actuator.

The aerodynamic results in terms of momentum in the chord direction for the downward and upward rotations of a traditional hinged aileron are depicted in Fig. 2. They were computed by 2D Reynolds–averaged Navier–Stokes (RANS) simulations, performed in SU2 [7], considering the airfoil section placed at the aileron root. The ±30 maximum rotation of the hinged aileron is evaluated at the design manoeuvring speed, indicated as V_A and characterized by Mach = 0.29 and zero altitude. It can be seen how these solutions are characterized by wide separation regions. It is expected that this situation can be improved thanks to the smooth curvature variation provided by morphing aileron.

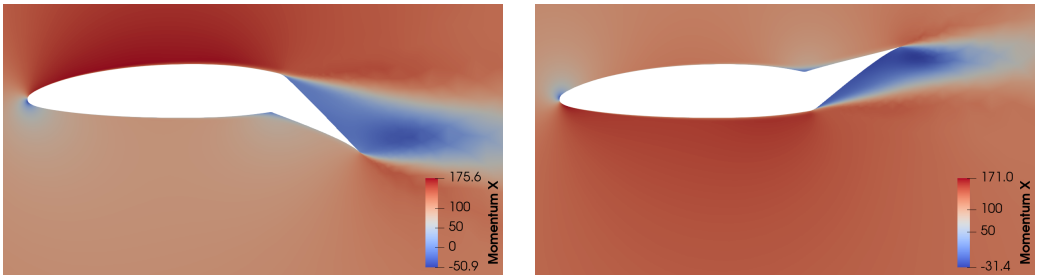

Fig. 2 Contour of the momentum in the chord direction for the hinged aileron.

The design of the morphing aileron is based on the morphing concept already presented and described in [8] the skin deformation allows for the deflection, while the actuation is introduced at the lower skin which is free to slide along the airfoil surface. Therefore, the actuation system consists of a linear sliding actuator connected to the lower skin. The sliding of the lower skin in both directions allows downward and upward morphing shapes to be achieved.

III. Morphing aileron shape optimization

One of the main difficulties in approaching shape–optimization is to select a suitable parameterization technique describing the wing geometry by a small but effective set of design variables. The method used in this work was originally proposed by Kulfan to perform aerodynamic shape optimization and to describe three–dimensional and analytically smooth geometries of several aircraft components, such as wing, body and nacelle. This method is called Class/Shape function Transformation (CST) technique [9] and it is based on merging a Shape Function with a Class Function. The Shape Function is composed by tunable components represented by the Bernstein polynomials, while the Class Function is a non–linear function that mathematically defines a basic wing shape. Some years ago, PoliMi has proposed an extension of this method able to identify an initial wing shape, starting from the original CAD model, and to introduce shape perturbations due to the morphing in a feasible way. Moreover, the structural behavior of the external skin can be reproduced analytically, without the need of FEAs [10].

A. Parameterization technique and optimization variables

A generic three–dimensional wing geometry can be mathematically defined as follows:

$$z(x, y) = c(\eta) \cdot \zeta(\psi, \eta)\,, \tag{1}$$

where $x = \psi \cdot c(\eta) + x_{LE}(\eta)$ and $y = \eta \cdot b/2$ are the dimensional coordinates obtained by multiplying the non–dimensional coordinates ψ and η by the local chord distribution $c(\eta)$ and the wing span b, respectively. The leading edge x position expressed as a function of η is described by $x_{LE}(\eta)$. The wing geometry is considered to be divided into an upper and a lower surface. Both non–dimensional surfaces can be described as follows:

$$\zeta(\psi, \eta) = C_{N2}^{N1}(\psi)\, \mathbf{Sy}_{(\mathbf{m},\mathbf{m})}(\eta) \cdot \mathbf{A}_{(\mathbf{m},\mathbf{n})} \cdot \mathbf{Sx}_{(\mathbf{n},\mathbf{n})}(\psi) + (1-\psi)\zeta_{LE}(\eta) + \psi\zeta_{TE}(\eta)\,, \tag{2}$$

where $\zeta_{TE}(\eta) = Z_{TE}(\eta)/c$ and $\zeta_{LE}(\eta) = Z_{LE}(\eta)/c$ are the trailing edge and the leading edge vertical position expressed as non–dimensional functions of η. The non–linear Class function is defined as $C_{N2}^{N1}(\psi) \triangleq \psi^{N1} \cdot (1-\psi)^{N2}$; the square matrix $\mathbf{Sy}_{(\mathbf{m},\mathbf{m})}(\eta)$ contains the Bernstein polynomial components of order m, which define a unit spanwise shape function, and the square matrix $\mathbf{Sx}_{(\mathbf{n},\mathbf{n})}(\psi)$ contains the Bernstein polynomial components of order n, which define a unit chordwise shape function. The rectangular matrix $\mathbf{A}_{(\mathbf{m},\mathbf{n})}$ is composed of the extra–coefficients acting in the spanwise and chordwise direction, respectively. Therefore, the Shape function is a two–dimensional function defined as: $\mathbf{S}(\psi, \eta) = \mathbf{Sy}_{(\mathbf{m},\mathbf{m})}(\eta) \cdot \mathbf{A}_{(\mathbf{m},\mathbf{n})} \cdot \mathbf{Sx}_{(\mathbf{n},\mathbf{n})}(\psi)$. Considering the matrix $\mathbf{A}_{(\mathbf{m},\mathbf{n})}$, each row defines a component

airfoil, and the first and last rows contain the extra–coefficients of the airfoils placed at the tips of the wing. The first and last columns are related to the leading and trailing edge boundary conditions and can be used to change their shape in the spanwise direction. When the CST technique is adopted to reproduce the shape changes due to the camber morphing, the square matrix can be partitioned into three sub–matrices: the first and last sub–matrices are related to the shape of the leading edge and the trailing edge, respectively, while the middle one is related to the shape of the wing–box. When the CST technique is used inside a shape optimization working on a leading edge or a trailing edge with morphing capabilities, the extra–coefficients of the first and last sub–matrices can be used as optimization variables. The extra–coefficients contained in the middle can be used to satisfy the shape constraints due to the presence of the wing–box, by a least–squares fitting. The mathematical formulation of this constraint represents the three–dimensional extension of the wing–box implicit constraint described in [10].

The CST parameterization technique described above is used to identify the original wing shape and then to introduce the shape changes due to the camber morphing.

In the case of the morphing aileron which is the subject of this study, the morphing shapes were parameterized using two design variables derived from the CST parameters. These variables are the trailing–edge equivalent rotation δ_{TE} and the airfoil boat–tail angle variation $\Delta\beta$, as depicted in Fig. 3. Even more variables could have been used, but these

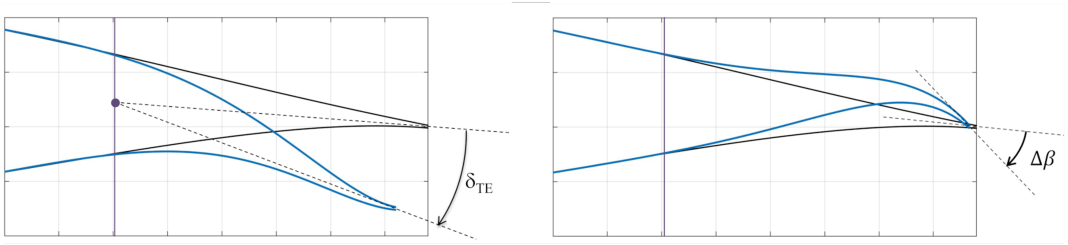

Fig. 3 Design variables used in this work to introduce shape changes due to the morphing.

two variables proved to be suitable for the description of the aileron shape changes due to the morphing.

The output of interests for the optimization are obtained from aerodynamic simulations and CST computations. On the one hand, the CST method can be also used to estimate the actuation energy or the actuation force. As will be described in the next section, in the case of a morphing device, the actuation energy is equal to the strain energy needed to change the shape of the skin plus the aerodynamic work needed to counteract the external forces.

On the other hand, lift and drag coefficients are computed with Reynolds–averaged Navier–Stokes (RANS) equations, solved in SU2, and the pressure coefficient distribution is used for the computation of the aerodynamic work performed with CST.

B. Structural and actuation aspects

After both the original and the morphing shapes are defined, the same parameterization technique is suitable to describe the structural behavior of the morphing skin. The first and second derivative of Equation 2 can be computed in a fully analytical way and this makes very efficient the calculation of the curvature $\kappa(x, y)$, at a generic point (x, y) of the wing geometry, and the length L of a portion of the wing geometry in a specific direction. Since the skin follows the external geometry of the wing, these quantities can be used to compute the axial strains ε_{axial} and bending strains ε_{bend} of the skin when the wing shape changes due to the morphing.

Although the concept of curvature can also be applied to the three–dimensional geometry of the wing, in the case of this work it is convenient to use the concept of curvature of a plane curve by defining specific directions as functions of the previously defined coordinates ψ and η. The reason is that the structural response is calculated starting from the curvature variation between two different three–dimensional surfaces, the undeformed and the morphing ones, and it is important that the curvature on the two surfaces is computed with respect to the same arc length.

Since the active camber morphing arises from a shape variation of the wing airfoils, it is convenient to use an arc length function l defined in the chordwise direction, then by the intersection between the surfaces describing the wing and a plane of principal curvatures parallel to the (x, z) plane. This means the existence of a parameterization $(x(l), z(l))$ such that the tangent vector $(x'(l), z'(l))$ has a norm equal to one and is thus a unit tangent vector. For example, in Fig. 4 the arc length l follows the upper skin of the morphing aileron and the lower skin is free to slide enabling the deformation of the aileron. Since the CST surfaces are at least twice differentiable, the curve obtained by

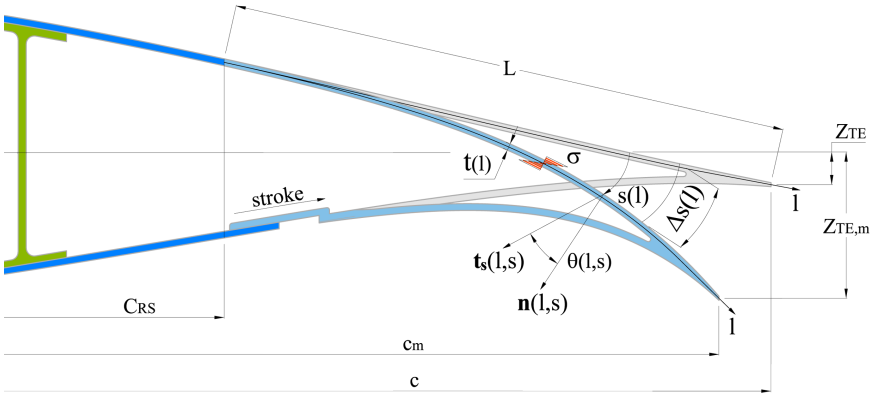

Fig. 4 Analytical quantities describing the morphing aileron behavior.

intersecting the surfaces with the plane containing the tangent vector is differentiable and the principal curvature on the airfoil planes can be computed as:

$$\kappa(l) = \sqrt{x''(l)^2 + z''(l)^2} = \frac{z''\left(x(l), \overline{y}\right)}{\left(1 + \left(z'(x(l), \overline{y}\right)^2\right)^{3/2}}, \tag{3}$$

where primes refer to derivatives with respect to l and $\overline{y}$ represents the spanwise location of the plane containing the tangent vector. The second formula of the Equation 3 enables a fully analytical evaluation of the curvature. In the case of a tapered wing or a deformation induced by a twisting skin, the component of principal curvature computed along η direction should be composed with the principal curvature computed along ψ direction. The component along η direction can be obtained through the curvature difference computed on the plane containing the tangent vector $(y'(l), z'(l))$.

When a morphing device is actuated, its external shape changes. The skin deformation is the result of its structural response and can be calculated in terms of stress σ or strain ε distribution over the skin surface. The strain, for example, can be considered as the combination of an axial and a bending component. The axial strain ε_{axial} is a simple function of the length variation ΔL calculated before and after the deformation, for a portion of the skin in the direction of interest. In the same way, the bending strain can be computed as a function of the curvature difference between the undeformed and the target surfaces. As mentioned above, the curvature on the two surfaces is computed with respect to the same arc length. If the arc length is defined in the chordwise direction, so by the intersection between the CST surfaces and a plane parallel to the airfoil sections, the curvature on the two surfaces can be calculated using Equation 3 and the curvature difference function is defined as follows:

$$\Delta\kappa(l) = \kappa_m\left(x(l)\right) - \kappa\left(x(l)\right), \tag{4}$$

where κ and κ_m are the curvature functions of the undeformed and the target surfaces, respectively. According to the Kirchhoff plate theory [11], the stress distribution σ, defined as a function of the arc length and the skin thickness, is shown in Fig. 4 and can be computed as:

$$\sigma_{bend}(l) = E \cdot \varepsilon_{bend} = E \cdot \tau(l) \cdot \Delta\kappa(l), \tag{5}$$

where E is the Young's modulus of the skin material, ε is the corresponding strain distribution and $\tau(l)$ represents a local coordinate perpendicular to the arc length, with origin in the centre line of the skin thickness. The maximum bending stress or strain along the arc length can be calculated as:

$$\sigma_{bend,max}(l) = E \cdot \varepsilon_{bend,max} = \frac{Et(l)}{2}\left(\Delta\kappa(l)\right), \tag{6}$$

where $t(l)$ is the skin thickness as a function of the arc length. The bending strain and stress generated when the skin is forced to assume the target shape, can be used for the computation of a part of the actuation energy.

According to the energy methods applied to structural analyses [11], the total actuation energy can be computed as a combination of the Strain Energy U, required to deform the morphing skin, and the Aerodynamic Work W_a, needed to counteract the aerodynamic forces [12]:

$$E_{tot} = U - W_a \,. \tag{7}$$

The energy is computed considering all parts of the skin. In the case of a trailing edge, for example, the contributions of both the upper and the lower skin are considered. Starting from the stress σ and the strain ε distribution of Equation 5, and according to the mathematical quantities shown in Fig. 4, the parameterization method can estimate the Strain Energy U as follows:

$$\begin{aligned} U &= \frac{1}{2}\int_{V_{skin}} \varepsilon \cdot \sigma \, dV = \frac{1}{2} E h \int_0^L \int_{-\frac{t}{2}}^{\frac{t}{2}} \varepsilon^2 \, d\tau \, dl = \\ &= \frac{1}{2} E h \int_0^L \Delta\kappa^2(l) \int_{-\frac{t}{2}}^{\frac{t}{2}} \tau^2 \, d\tau \, dl = \frac{1}{2} E h \int_0^L \frac{t^3(l)}{12} \Delta\kappa^2(l) \, dl \,, \end{aligned} \tag{8}$$

where L is the skin length along the arc length, V and V_{skin} is the volume of the skin and h is the skin length in spanwise direction. Equation 8 for the strain energy calculation is general, but it is here simplified assuming that the morphing aileron, and all its structural properties are constant in the spanwise direction.
The work performed by aerodynamic forces during morphing deformation W_a can be computed as:

$$\begin{aligned} W_a &= \int_0^{\Delta s(l)} \int_{A_{skin}} p(l,s) \, d\mathbf{A} \cdot \, d\mathbf{s} = \\ &= \int_{V_{morph}} p(l,s) \, \mathbf{n} \cdot \mathbf{t_s} \, dv = h \int_0^L \int_0^{\Delta s(l)} p(l,s) \, \mathbf{n} \cdot \mathbf{t_s} \, ds \, dl = \\ &= \frac{1}{2} h \int_0^L \left(\, p_0(l) \cos\left(\theta_0(l)\right) + p_T(l) \cos\left(\theta_T(l)\right) \right) \, \Delta s(l) \, dl \,, \end{aligned} \tag{9}$$

where A and A_{skin} is the skin surface area and v and V_{morph} is the volume generated by the skin during the deformation due to the morphing. All other quantities are shown in Fig. 4. The unit vector $\mathbf{n}(l,s)$ is normal to the skin surface, while the unit vector $\mathbf{t_s}(l,s)$ is tangent to the displacement $s(l)$ of each point along the skin during deformation. Each of these points forms a path of length $\Delta s(l)$. The dot product $\mathbf{n} \cdot \mathbf{t_s}$ is equal to $\cos(\theta(l,s))$, where $\theta(l,s)$ is the angle between $\mathbf{n}$ and $\mathbf{t_s}$. When the skin is undeformed $\theta_0(l) = \theta(l,0)$, while $\theta_T(l) = \theta(l, \Delta s(l))$ when the skin achieves the target shape. The last step of Equation 9 is valid under the assumption of linear variation of the pressure distribution $p(l,s)$ acting on the skin during deformation. The initial pressure distribution $p_0(l)$, acting on the skin when it is undeformed, becomes $p_T(l)$ when the skin is deformed and achieves the target shape. The CST technique can be coupled with any aerodynamic solver to compute pressure distributions $p_0(l)$ and $p_T(l)$. Thanks to its analytical nature, the CST formulation is used for directly generating the aerodynamic mesh, saving computational time in the pre–processing phase.

What is important to point out is that the total actuation energy E_{tot} is valid for any actuator installed inside the morphing device, while the actuation force depends on the position of the actuator and depends on the actuator stroke. Therefore, the actuation force can be minimized looking for a morphing shape which minimizes the total energy or maximizes the actuator stroke. Assuming the linear slider of Fig. 4 connecting the bottom skin to the rear spar, the actuator stroke can be easily computed because we know, for example, how much the lower skin becomes shorter when the aileron deflect downwards. According to a linear relationship between actuation force and actuator stroke, the maximum actuation force achieved during aileron deployment can be estimated starting from the actuation energy.

C. Optimization problem definition

The procedure for the design of morphing aileron proposed in this article consists of a design optimization aimed at the defining of the most efficient shape, in terms of aerodynamic drag and required actuation force, subject to aerodynamic and structural constraints that account for the structural behaviour of the morphing skin, respectively. The CST technique

and the total energy computation described in Section III.B are embedded into the optimization procedure and used to minimize the maximum linear force F_{act}. The maximum linear force is computed starting from the static force needed to keep fixed the aileron in the undeformed condition, under the corresponding aerodynamic loads. Then, the peak force can be calculated starting from the integral of the force that must be equal to the total energy E_{tot}, assuming a linear trend as a function of the actuator stroke. According to the kinematic solution described in Section II, i.e. a linear slider connecting the bottom skin to the fixed part of the wing, the actuator stroke can be computed as the variations in the lower skin length. Constraints limiting the structural response of the skin are based on a Constant Cross–section Length (CCL) strategy that forces the skin to keep the axial strain ε_{axial} equal to zero and the bending stress under the allowable limit of the material. This strategy does not require finite element analyses, because the stress or strain computation is embedded into the CST formulation described in Section III.A, and allows that also the aerodynamic analyses are performed only on feasible morphing shapes.

The optimization scheme consists of two nested optimization loops: the inner one produces only feasible morphing shapes, the outer one performs the aerodynamic evaluation. In this way, only morphing shapes that meet all the structural and mechanical constraints, are considered during the aerodynamic computation. The shape optimization is formulated as a multi–objective problem:

$$\begin{aligned} \min_{\mathbf{x}=\{\delta_{TE};\,\Delta\beta\}} \quad & \{F_{act}(\mathbf{x});\; C_d(\mathbf{x})\} \\ \text{such that} \quad & C_l(\mathbf{x}) \geq C_{l,\,Required} \\ & \varepsilon_{axial,\,Up} = 0 \\ & \max\left(\Delta\kappa(\mathbf{x})\right) \leq \overline{\Delta\kappa} \\ & \mathbf{x}_{low} \leq \mathbf{x} \leq \mathbf{x}_{up} \end{aligned} \tag{10}$$

where $\mathbf{x} = \{\delta_{TE}; \Delta\beta\}$ are the design variables, whereas drag coefficient C_d and actuation force F_{act} are objectives to minimize. The lift coefficient C_l is constrained to be greater than or equal to the required lift coefficient $C_{l,\,Required}$. The other constraints prevent axial stresses in the upper skin, limit the actuator stroke and limit the maximum curvature variation. The uncertainty associated to the absence of structural design in this phase, in particular the thickness distribution of the skin that affects the strain energy contribution, can be handled by parametrically solving the optimization problem for different thickness values.

The result of this multi–objective optimization is a Pareto front that shows how drag coefficient and actuation force are conflicting requirements. Several candidate shapes can be selected for the subsequent steps of analysis and design. The described procedure is a single–point shape optimization, characterized by a single flight condition and a single deflection level. The procedure can be repeated to find shapes corresponding to different levels of deflection. These shapes will then be used for the multi–point structural design of the morphing aileron.

D. Optimization results and morphing aileron shapes

The optimization problem described with Equation 10 is solved by using a Design of Experiments (DOE) approach based on the response surface method (RSM). This approach offers the great advantage of not having to perform aerodynamic analyzes during the optimization process. After creating a database of aerodynamic results, it is then possible to repeat the optimization many times by varying parameters such as the constraint values or even the optimal problem formulation, with a great time saving.

1. Shape optimization results

Surrogate models of the objective and constraints functions are built using a Radial Basis Function (RBF) interpolation. The outputs of interest can be computed for a Latin hypercube sample in the space of the design variables shown in Fig. 3 and the obtained values used to construct the response surface approximation models. The design points for the DOE approach are represented in Fig. 5, for both the downward and upward deflection cases.

For each point, the CFD RANS analyses are performed at Mach = 0.29, 0 m altitude and Angle of Attack AoA = 2.0 deg, considering the airfoil placed at the root section of the aileron region. Starting from the aerodynamic results computed on both the baseline airfoil and the airfoil shape obtained acting on the design variables, the actuation force needed to obtain this shape variation is calculated in a semi–analytical way using the methodology described in Section III.B. The obtained results are used to construct the response surfaces of interest. Figure 6 represents the response surface for lift

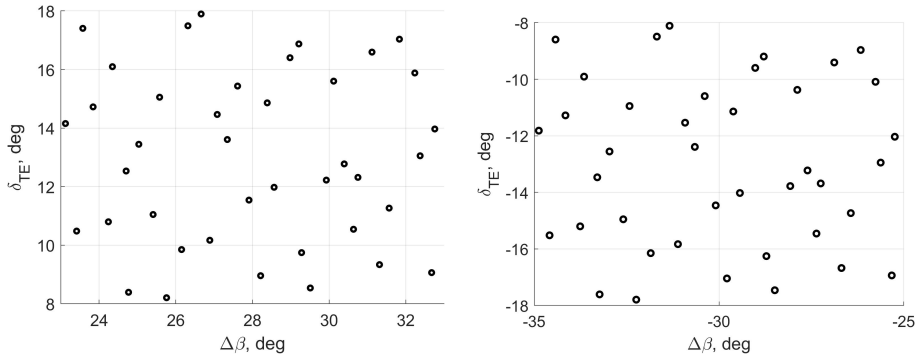

Fig. 5 Latin hypercube samples in the space of the design variables.

coefficient, drag coefficient, and actuation force, in the downward deflection case. The same results for the upward deflection case are reported in Fig. 7.

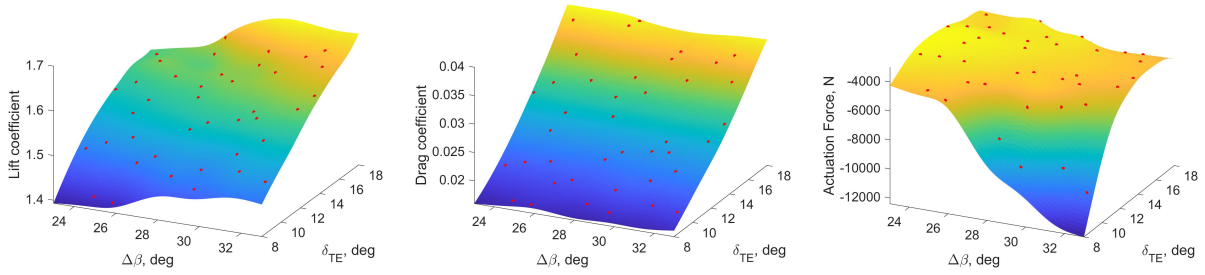

Fig. 6 Response surfaces used for the shape optimization of the downward deflected morphing aileron.

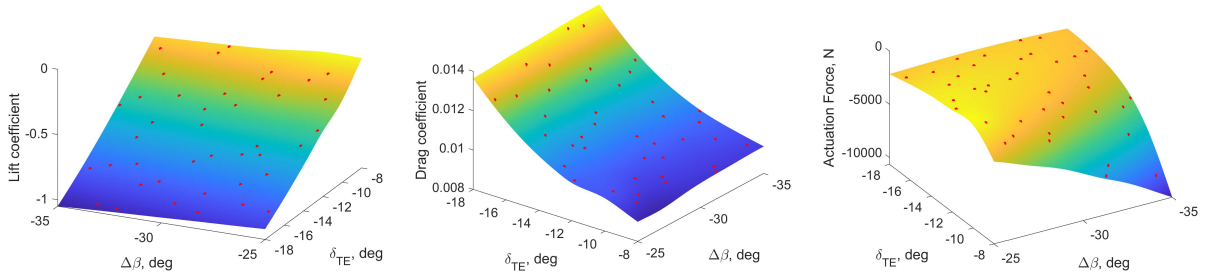

Fig. 7 Response surfaces used for the shape optimization of the upward deflected morphing aileron.

The optimization problem stated in Equation 10 is solved using the obtained responses and the following constraint values: $C_{l,\,Required}$ has been set to a value corresponding to lift variations of 125% and -215%; the maximum curvature variation $\overline{\Delta\kappa}$ has been set to 6 $\frac{1}{m}$, according to a skin made of composite material; bounds to be assigned to the design variables have been set according to the Latin hypercube sample.

Since the multi–objective optimization finds multiple optimal solutions, at the end of the process, the optimal shape solution can selected from a Pareto Front, establishing how much to make the actuation force objective prevail over that on the aerodynamic drag. The Pareto front obtained for the downward deflection is shown in Fig. 8, together with the relationship between the corresponding optimum design variables. Three different solutions are highlighted in this Figure, and the corresponding morphing shapes are represented in Fig. 9.

Analogous results are reported for the shape optimization of the upward deflection. The Pareto front is shown in Fig. 10 and the corresponding optimum design variables are also reported. Three different solutions have been selected, and the corresponding morphing shapes are reported in Fig. 11.

The selection of the optimal shape was made using the force minimization as the main design criterion. However this shape represents a Pareto point so it also minimizes the aerodynamic drag. Indeed, the polar curves shown in Fig. 15

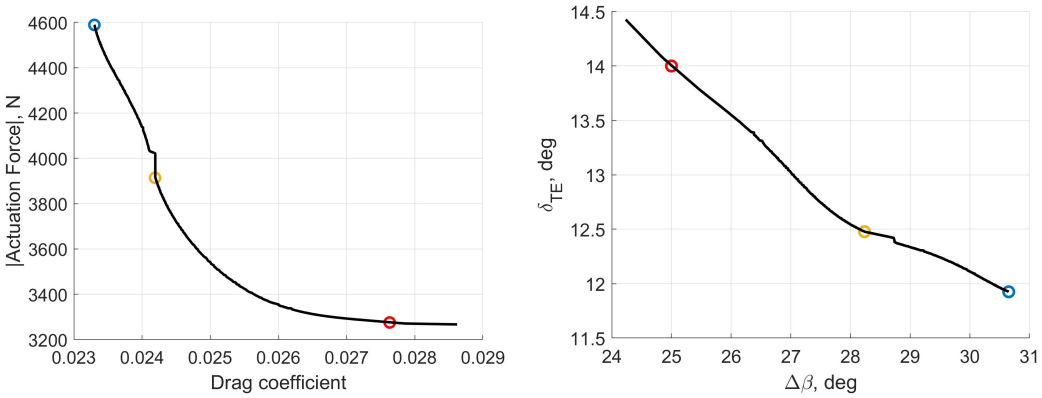

Fig. 8 Shape optimization results for the downward deflected morphing aileron.

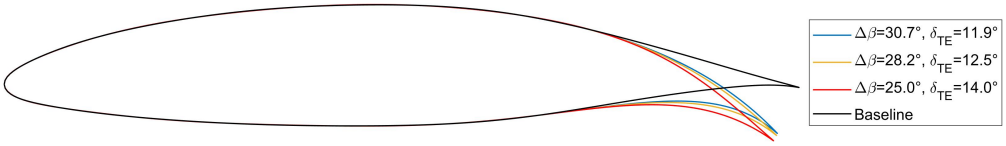

Fig. 9 Three different downward deflected aileron shapes from the Pareto front of the shape optimization.

show a big benefit also in terms of aerodynamic drag, despite having selected the design point in the lower part of the pareto fronts. The selected optimum morphing deflections, which correspond to the red points and the red shapes, are illustrated in Fig. 12, compared with the rotations of the traditional aileron. The comparison with the hinged solutions rotated by ±30 deg is reported for both the root section and the tip section.

The curvature variation distribution for the selected morphing shapes can be computed by the CST technique, as explained in Section III.B, and it is reported in Fig. 13 for both the downward and upward deflections. Strain values in the skin depends on the curvature variation and the skin thickness. Assuming a maximum thickness of 3.5 mm, which is a reasonable choice according to the results that will be shown in the Section IV, the maximum bending strain corresponding to $\Delta\kappa = 2$ is 0.35%, which is compatible with the allowable values of any aeronautical material.

In this regard, the authors want to highlight clearly that, in this design phase, it is not important to know the correct thickness distribution of the skin because the goal is to define the optimal morphing shape such as to minimize the actuation force, together with the aerodynamic drag, whatever the thickness values that will be found below

The aerodynamic characteristics of the selected optimal morphing shapes are shown here in terms of contours of the momentum in the chord direction and polar curves. The aerodynamic momentum for both the downward and upward deflections is depicted in Fig. 14. These results, compared with those in Fig. 2, show how the morphing allows to avoid

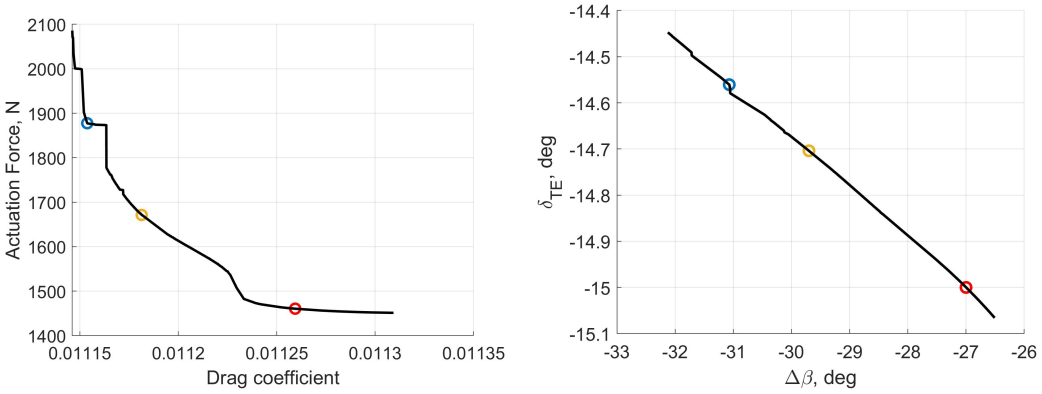

Fig. 10 Shape optimization results for the upward deflected morphing aileron.

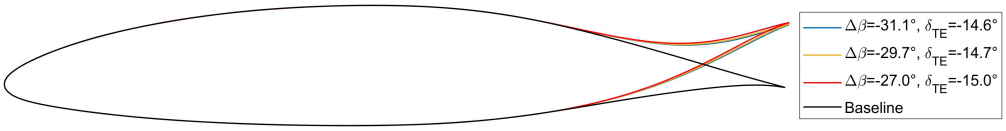

Fig. 11 Three different upward deflected aileron shapes from the Pareto front of the shape optimization.

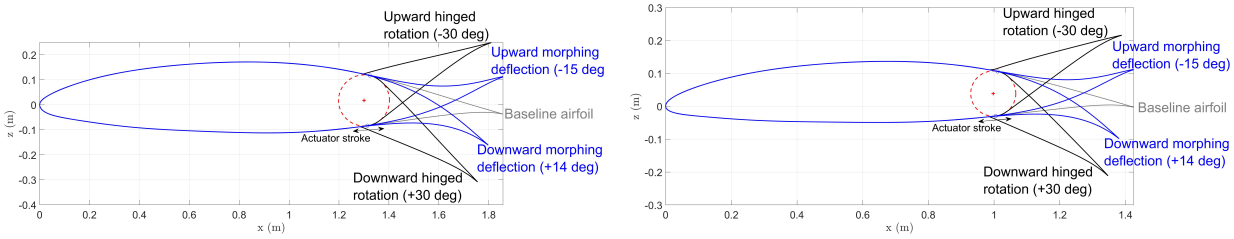

Fig. 12 Comparison between morphing and hinged aileron shapes: root section (left) and tip section (right).

or at least greatly limit the flow separation and the detachment of the boundary layer.
The overall aerodynamic benefit of the morphing aileron with respect to the conventional hinged aileron is explained by the comparison of the aerodynamic performances of morphing and hinged aileron, as shown in Fig. 15. The morphing solutions are characterized by less drag to achieve the required lift coefficient. Moreover, while the upward hinged aileron stalls for angles of attack lower than -2 deg, the corresponding morphing solution delays the stall by 4 deg making it much more gradual.

The pair of optimal values assigned to the design variables were propagated along the wingspan to all airfoils included in the aileron region, obtaining the three–dimensional optimal morphing shapes in the case of the downward and upward aileron deflection for its maximum deployment. The corresponding 3D CST models are shown in Fig. 16. The CST technique enables the computation of the deformation trajectory length for each point of the skin. The displacement evaluated at the lower skin in the reference position of the slider corresponds to actuator stroke requirement. The required strokes at the root section of the aileron are -45 mm and 49 mm for the downward and upward morphing deflections, respectively. The former requires a pushing actuation force, whereas the latter requires a pulling force. The corresponding values at the tip section of the aileron are -31 mm and 33 mm. These results represent a preliminary information for the selection of the actuator.

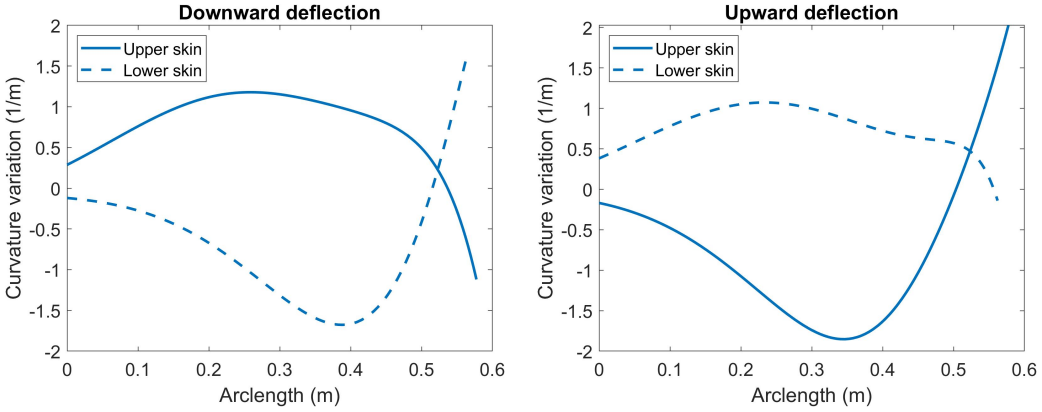

Fig. 13 Curvature variation for the downward (left) and upward (right) morphing deflections.

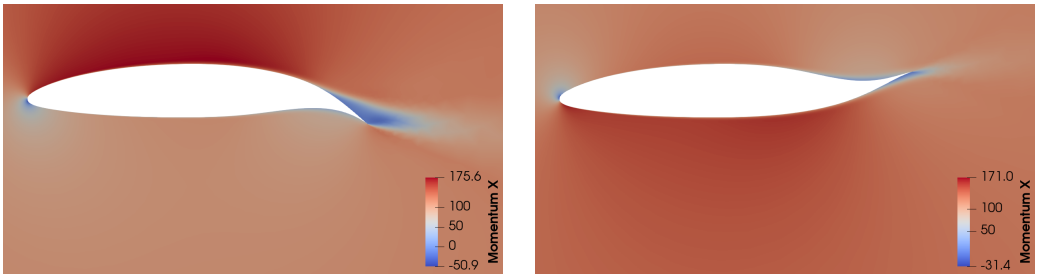

Fig. 14 Contour of the momentum in the chord direction for the morphing aileron.

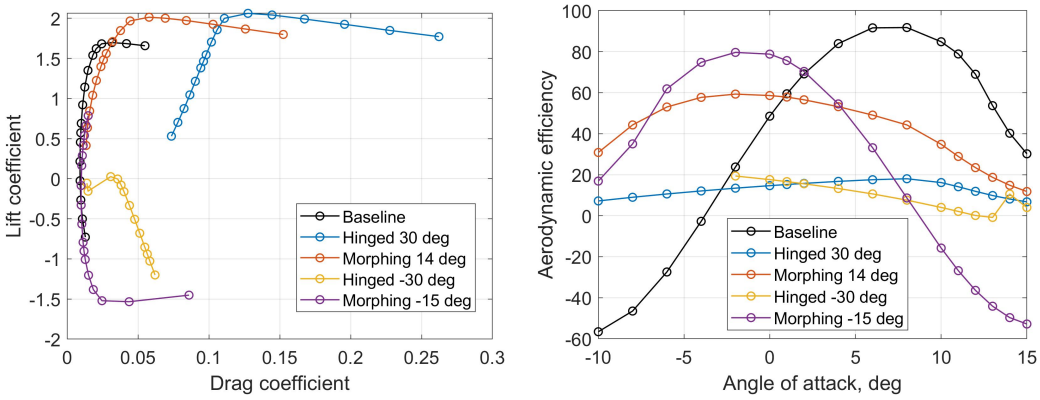

Fig. 15 Aerodynamic comparison between morphing and hinged aileron in terms of polar curves (left) and aerodynamic efficiency as a function of the Angle of Attack (right).

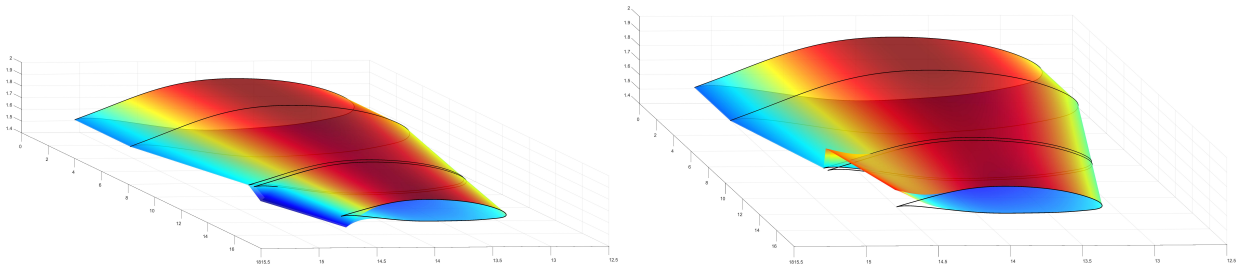

Fig. 16 3D CST models representing the optimal downward and upward deflections of the morphing aileron installed on the reference wing.

IV. Preliminary design of the aileron compliant structure

The procedure adopted in this work for the structural design of the morphing aileron includes an in–house design tool which leads to the design of a compliant structure based on the distributed compliance concept, where only flexible elements are used instead of rigid mechanical components. This tool consists of a topology optimization coupled with non–linear finite element analyses and a dedicated multi–objective Genetic Algorithm.

A. Aileron structural configuration and design variables

The genetic algorithm works on three different types of design variables that are strictly related to the aileron structural configuration which involves the use of secondary spars connecting the upper and lower skin:

1) the skin thickness distribution;
2) the location of the end points of a variable number of flexible spars connecting the upper and lower skin;
3) the thickness of each internal spar.

The non–linear finite element analyses are performed on a medium–fidelity FEM model represented in Fig. 17 which is automatically generated at each optimization step. The adopted model represents a limited spanwise section of the device, thus avoiding 3D effects, that will be considered at a later stage of the design process. The structural optimization

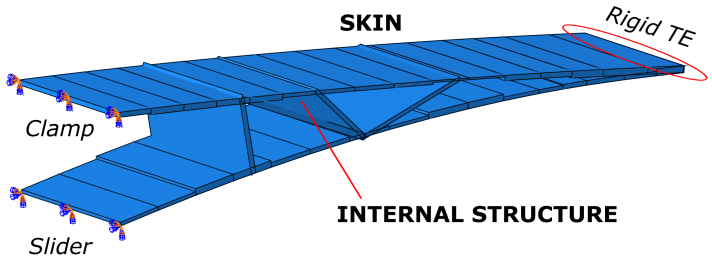

Fig. 17 FEM model used for the topology and sizing optimization of the morphing aileron.

consists of a topology and sizing genetic algorithm based on dedicated crossover and mutation functions enabling to combine topology, sizing and shape design variables into the same optimization process. For example, the mutation can act on binary variables turning on or off each internal spar. At the same time, both the mutation and the crossover can change the skin cross–sectional sizes, as well as the spar thicknesses, or the position of the points connecting the skin with the internal spars. Figure 18 shows a possible modification of the structural configuration through the application of these functions, where the points connecting the skin with the internal spars are called beam destinations.

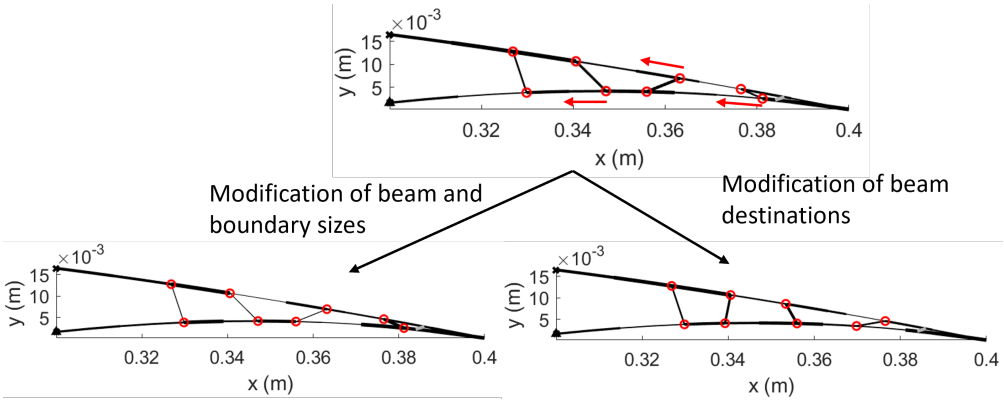

Fig. 18 A demonstrative connected representation of a compliant morphing aileron.

B. Multi–objective design optimization

Different objective functions can be considered during the topology optimization:

- Kinematic requirement: the Least Square Error (LSE) between the Target shapes (Maximum Upward and Downward deflections previously defined by the shape optimization) and the skin deformation computed by non–linear finite element analyses, when the mechanism is actuated under the aerodynamic loads corresponding to Mach = 0.29 and 0 m altitude, for the downward deflection (AoA = 8 deg) and the upward deflection (AoA = -4 deg);
- The actuation force, computed by non–linear finite element analyses, while imposing the actuation stroke (previously defined by the shape optimization) on the linear slider, connecting the bottom skin to the rear spar, to allow the mechanism to achieve the upward or the downward deflections, under corresponding aerodynamic loads;
- Structural requirement: the Least Square Error (LSE) between the undeformed airfoil shape and the skin deformation computed by linear finite element analyses when the mechanism is not actuated, under the most critical design condition corresponding to Mach = 0.45 and 0 m altitude (AoA = 4 deg).

Moreover, a requirement on the frequency of the first mode of the structure, which is required to be greater than or equal to 20 Hz, can be included to guarantee a dynamic behavior compatible with the desired bandwidth.

In the case of a multi–point structural design, the kinematic LSE and the actuation force objectives can be included for each of the shapes of interest. Thanks to the multi–objective approach, the genetic algorithm will try to find a trade–off in achieving differently deflected shapes. In the case of this work, 2 kinematic requirements are considered corresponding to the upward deflection and the downward deflection of the aileron. Since the multi–objective Genetic Algorithm finds multiple optimal solutions, at the end of the process the optimal topology solution can be selected from a Pareto Front, taking into account manufacturing requirements which are not included in the optimization problem. The designer can select different structural solutions for the subsequent validation phase, starting from the aerodynamic analyses of the obtained morphing deformation to assess if the target lift coefficients are achieved.

C. Optimization results and selected design points

The described procedure is applied on the wing section located at 2 meters from the wing tip. For this section, the estimated stroke values are -37.1 mm and 37.5 mm, for the downward and upward morphing deflections respectively. These values are used to perform imposed–displacements non–linear finite element analyses during the execution of the genetic algorithm.

The structural optimization problem is initially solved considering the minimization of the LSE for the three design conditions and then adding the minimization of the actuation force, which is calculated as a constrain force in the slider inserted on the lower skin. The optimization result in terms of Pareto front is represented in Fig. 19.

The highlighted solution is selected and the corresponding structural configuration is shown in Fig. 20. In the same figure, the 3D deformations, related to both the downward and upward deflection, are depicted together with the contour of the maximum principal strains computed by the solver Abaqus.

What may be interesting to point out is that strain limits are satisfied and the strain values obtained by these finite element analyzes are compatible with the estimate that had been obtained geometrically, via the CST technique, during the shape design, i.e. from graphs in Fig. 13.

The results coming from finite element analyses are also used to compare the deformation and the target shapes coming from the shape optimization, so from the results of Fig. 12. The comparison in the case of downward and upward deflection, is reported in Fig. 21.

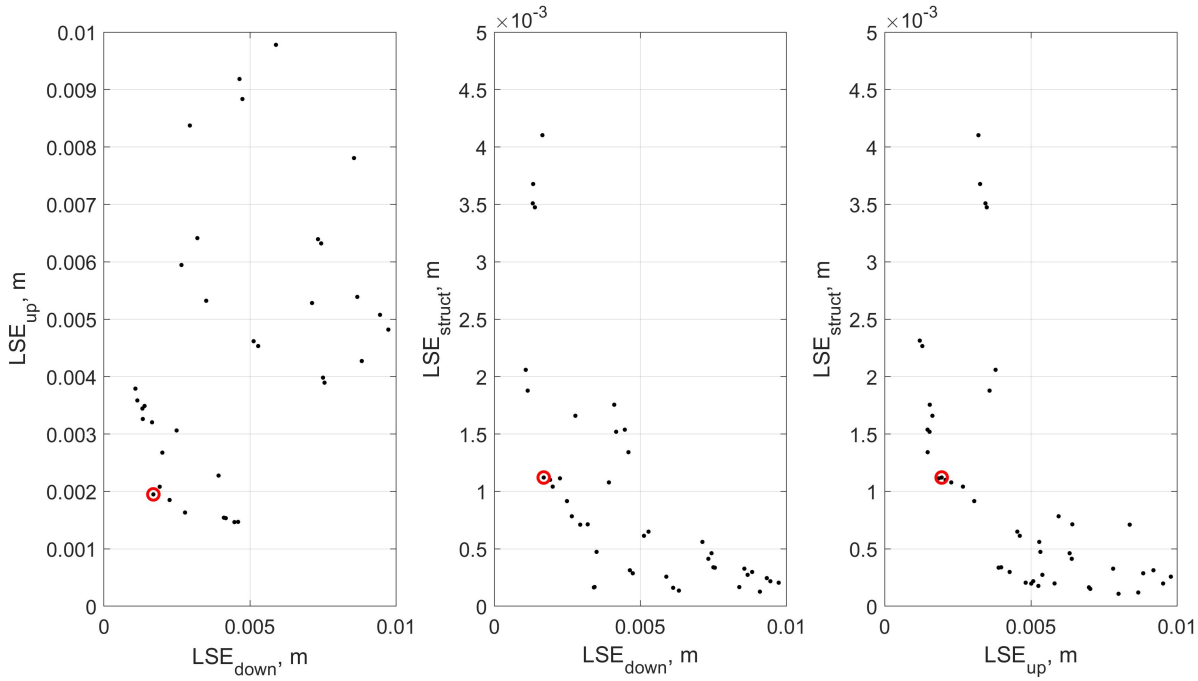

Fig. 19 Pareto front from the structural optimization.

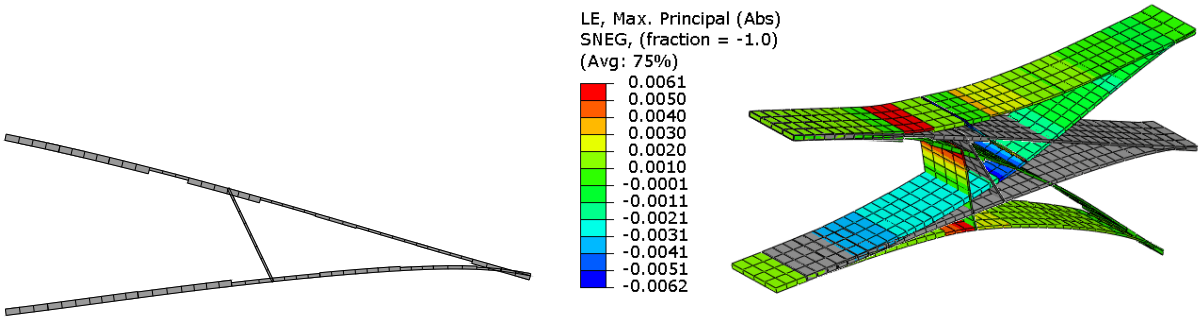

Fig. 20 Structural configuration and finite element results.

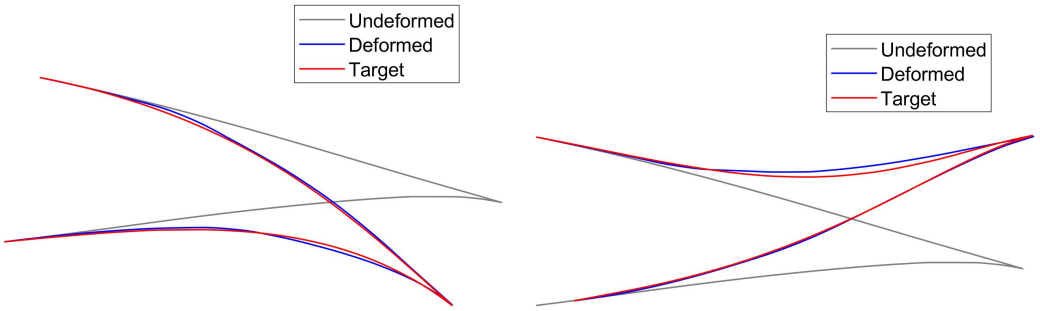

Fig. 21 Comparison between deformed and target shapes for the solution.

V. Performance assessment

The validation of the morphing aileron includes the aerodynamic analysis of the deformed shape, achieved during finite element analyses, to verify that the lift coefficient requirements are satisfied by the designed structural solution. Moreover, the comparison between the hinged and the morphing solution is performed in terms of actuation requirements and aerodynamic performances.

Starting from the first assessment, the designed structural solution is validated from the aerodynamic viewpoint. To this end, the CFD analyses of the achieved deformed shapes are performed and the results are compared with those of the target shapes. This comparison shows small differences in terms of lift and drag coefficients. The pressure coefficient distribution for the target shapes and the deformed shapes are compared in Fig. 22.

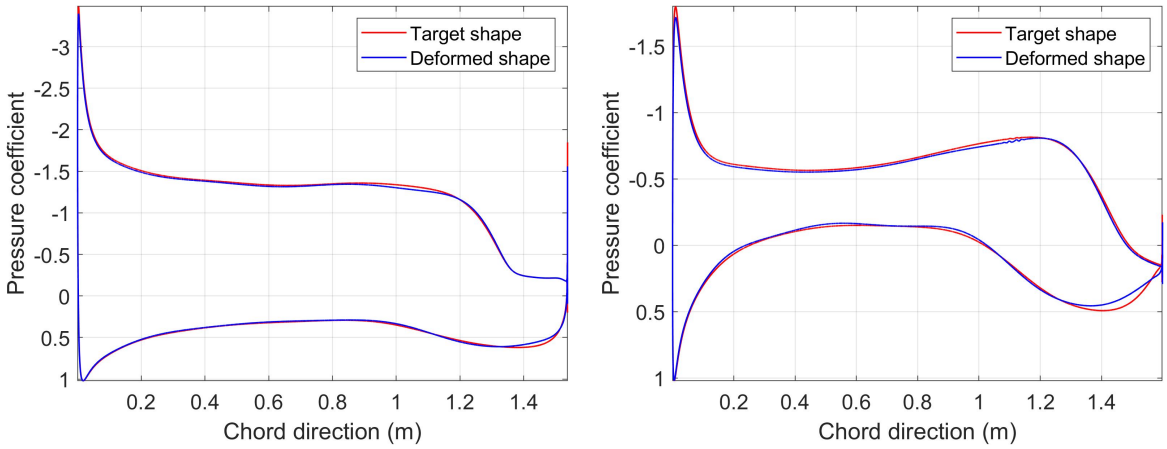

Fig. 22 Comparison of pressure coefficient distributions at AoA = 2 deg for the downward (left) and upward (right) morphing deflections.

Once the aerodynamic performances of the designed morphing solution are validated, these results can be compared with the corresponding hinged solutions from both the aerodynamic and actuation force viewpoint. The actuation force required for the morphing aileron consists of a structural contribution to perform the morphing process and an aerodynamic contribution to counteract the external aerodynamic loads. The total actuation forces required for the morphing aileron are obtained from the FEM analyses performed on the designed solution. The actuation force for the hinged aileron is totally due to aerodynamic loads. This force is estimated from the hinge moment computed on the rigidly rotated aileron, assuming an internal leverage. The comparison between conventional hinged aileron and the designed morphing aileron is reported in Fig. 23, in terms of drag coefficient and actuation force. Absolute values for

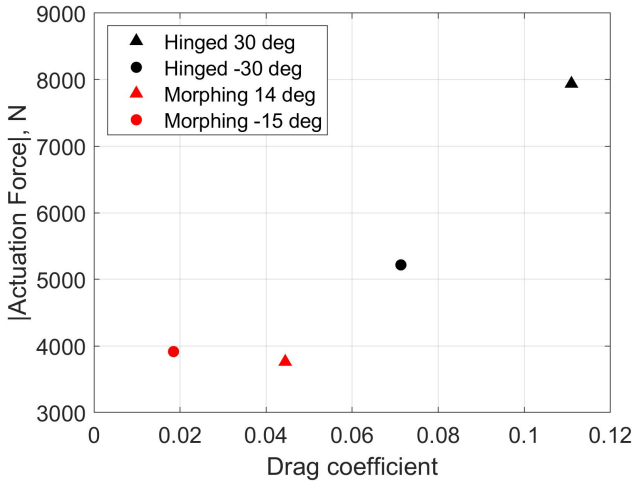

Fig. 23 Comparison of aerodynamic and actuation performances between hinged and morphing aileron.

the actuation forces are reported in Fig. 23. However, it must be remembered that downward and upward deflections require opposite sign for the force, corresponding to pushing and pulling forces respectively.

Although there is a strain energy contribution associated with the morphing process, the actuation force for the morphing aileron is lower than the force required by hinged solutions. It is possible to achieve this outcome because the morphing aileron shapes provide the target lift coefficient with smaller trailing–edge equivalent rotation compared to the rigid rotation of the hinged aileron. Therefore, the designed morphing aileron overcomes the conventional aileron from both the aerodynamic performance and the actuation requirement viewpoints.

Finally, the dynamic behavior of the morphing aileron is preliminarily investigated performing the modal analysis of the designed structure. The first mode shape is represented in Fig. 24. The corresponding modal frequency is 59 Hz. This frequency value is high enough to exclude coupling between structural dynamics and actuator bandwidth, which should not exceed 10 Hz.

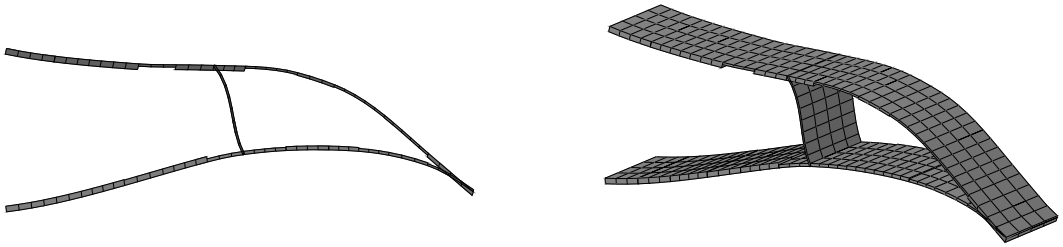

Fig. 24 First mode shape for the designed structural solution.

VI. Conclusion

This paper has described the optimization procedure for the design of a morphing aileron in the framework of HERWINGT project. First, shape optimization is adopted to determine candidate target shapes considering aerodynamic, structural, and actuation requirements. Second, the structural design is performed to obtain structural solutions able to achieve the target shapes. Finally, aerodynamic, actuation, and dynamic evaluations are presented for the validation of the designed concept and to compare the traditional hinged aileron with the designed morphing aileron which has proven to be superior both from the point of view of the required actuation force and aerodynamic drag.

VII. Acknowledgements

This project has received funding from the Clean Aviation Joint Undertaking under grant agreement No. 101102010. The granting authority receives support from the European Union's Horizon Europe research and innovation programme and the Clean Aviation Joint Undertaking members other than the Union.

VIII. Disclaimer

Funded by the European Union. Views and opinions expressed are however those of the author(s) only and do not necessarily reflect those of the European Union or Clean Aviation Joint Undertaking. Neither the European Union nor the granting authority can be held responsible for them.

References

[1] European Commission and Directorate-General for Mobility and Transport and Directorate-General for Research and Innovation, *Flightpath 2050: Europe's vision for aviation : maintaining global leadership and serving society's needs*, Publications Office,

2011. https://doi.org/doi/10.2777/50266.

[2] Monner, H., Kintscher, M., Lorkowski, T., and Storm, S., "Design of a smart droop nose as leading edge high lift system for transportation aircrafts," *50th AIAA/ASME/ASCE/AHS/ASC Structures, Structural Dynamics, and Materials Conference 17th AIAA/ASME/AHS Adaptive Structures Conference 11th AIAA No*, 2009, p. 2128.

[3] Woods, B. K., Bilgen, O., and Friswell, M. I., "Wind tunnel testing of the fish bone active camber morphing concept," *Journal of Intelligent Material Systems and Structures*, Vol. 25, No. 7, 2014, pp. 772–785.

[4] Weisshaar, T. A., "Morphing aircraft technology-new shapes for aircraft design," 2006.

[5] De Gaspari, A., and Ricci, S., "A Two–Level Approach for the Optimal Design of Morphing Wings Based On Compliant Structures," *Journal of Intelligent Material Systems and Structures*, Vol. 22, No. 10, 2011, pp. 1091–1111. https://doi.org/10.1177/1045389X11409081.

[6] De Gaspari, A., "Multiobjective Optimization for the Aero-Structural Design of Adaptive Compliant Wing Devices," *Applied Sciences*, Vol. 10, No. 18, 2020, p. 30. https://doi.org/10.3390/app10186380.

[7] Sanchez, R., Palacios, R., Economon, T. D., Kline, H. L., Alonso, J. J., and Palacios, F., *Towards a Fluid-Structure Interaction Solver for Problems with Large Deformations Within the Open-Source SU2 Suite*, 2016. https://doi.org/10.2514/6.2016-0205, URL https://arc.aiaa.org/doi/abs/10.2514/6.2016-0205.

[8] De Gaspari, A., Riccobene, L., and Ricci, S., "Design, Manufacturing and Wind Tunnel Validation of a Morphing Compliant Wing," *Journal of Aircraft*, Vol. 55, No. 6, 2018, pp. 2313–2326. https://doi.org/10.2514/1.C034860.

[9] Kulfan, B. M., "Universal Parametric Geometry Representation Method," *Journal of Aircraft*, Vol. 45, No. 1, 2008. https://doi.org/10.2514/1.29958.

[10] De Gaspari, A., and Ricci, S., "Knowledge–Based Shape Optimization of Morphing Wing for More Efficient Aircraft," *International Journal of Aerospace Engineering*, Vol. 2015, 325724, 2015, pp. 1 – 19. https://doi.org/10.1155/2015/325724.

[11] Bauchau, O. A., and Craig, J. I., *Structural Analysis: With Applications to Aerospace Structures*, Solid Mechanics and Its Applications (SMIA, volume 163), Springer Science & Business Media, 2009. https://doi.org/10.1007/978-90-481-2516-6.

[12] De Gaspari, A., "Study on the Actuation Aspects for a Morphing Aileron Using an Energy–Based Design Approach," *Actuators*, Vol. 11, MDPI, 2022, p. 185.